Molecular Dynamics Simulations of Water with Novel Shell-Model Potentials

Paul J. van Maaren and David van der Spoel*

Department of Biochemistry, Uppsala University, Husargatan 3, Box 576, 75123 Uppsala, Sweden

Received: October 18, 2000; In Final Form: January 11, 2001

The need for a computationally efficient yet physically realistic water model for molecular simulation is longstanding. To account for intermolecular interactions with other molecules, for example the hydration of biomolecules, the model has to be able to adapt itself to different environments. To this end, a number of water models have been proposed that incorporate polarizability with varying degrees of success. We have developed new water models, flexible as well as rigid, on the basis of the shell concept, with three atoms and an extra particle representing the electronic degrees of freedom. This particle is coupled to a dummy position on the bisector of the molecule by a harmonic spring. We named the models SW, or shell water models. To account for anisotropic polarization, the spring force on the shell particle has been modified to depend on the displacement of the shell particle in the molecular coordinate frame. The model is constructed so as to reproduce the vacuum dipole and quadrupole, and the spring constants are chosen such that the polarizability, be it isotropic or anisotropic, is consistent with experimental data. Then the Lennard-Jones parameters are optimized to reproduce the liquid energy and density. The model is evaluated by checking liquid- and gas-phase properties, and the influences of anisotropy and flexibility are discussed.

1. Introduction

Water has been called "the lubricant of life" because of its proposed role in mediating extremely fast conformational fluctuations in peptides.[1] The picosecond time scale of such motions as detected by Raman optical activity[2] makes them tractable for further study using molecular dynamics (MD) simulation, and similar fast fluctuations in peptide backbone conformation have indeed been found in MD simulations of short peptides.[3] However, the accuracy of modeling water−peptide interactions is still a matter of concern, and it has even been questioned whether computer simulations of water contain any predictive power at all.[4] In a previous study on solvated peptides where several water models and peptide force fields were compared,[5] we found that with the extended simple point charge water model (SPC/E[6]) most of the experimental NMR data on these peptides[7] could be reproduced. However, in some of the simulations the built-in polarization correction of the SPC/E model makes it too hydrophilic, an effect which has also been observed in interface simulations.[8] From these observation we can conclude that the SPC/E is not the ideal water model for solvation studies. For the bulk solvent it is an excellent model, which is demonstrated by the fact that many of the bulk properties are reproduced in computer simulations of SPC/E water.[9−11]

It is now well established that in order to treat solvation reliably it is necessary to include polarizability in the potential energy function. An example of such a model is the modified simple point charge model (SPC[12]), where an isotropic point polarizability was added to the oxygen atom.[13] In this model the charges on the atomic sites were chosen so as to reproduce the vacuum dipole. The model was able to capture some of the properties of water like rotational correlation times, but overall it was not better than SPC/E for bulk water. Subsequently, other models were proposed on the the basis of the same principles of three charged sites and a point polarizability.[14−21] These models are a genuine improvement on the older models because the Lennard-Jones parameters as well as the charges have been optimized to reproduce critical observables.

One particularly successful water model, the fluctuating charge (FQ) model of Berne and co-workers,[22] is of quite another nature. In this model the charges on the atoms fluctuate in response to the local electric field under the constraint of neutrality. The model has an important conceptual deficiency, however, in that it cannot change its polarization out of the plane of the molecule because the charges are confined to the atomic positions. This contrasts the fact that the polarizability of water is nearly isotropic, i.e., the same in all directions. Despite this, the overall quality of the model, which is its ability to reproduce properties in agreement with experimental observations, is remarkable. The FQ methodology has recently also been applied to amino acids solvated in water.[23] In that work, the OPLS potential function[24] was used for the peptide, and the charges were allowed to fluctuate in the peptide as well as the water molecules. For a FQ model of (planar) aromatic compounds it turned out to be necessary to add fluctuating dipoles, to reproduce the out of plane polarizability.[25]

Our aim is to make a phase transferable water model, like we have done successfully for the N_2 molecule.[26] The strategy is to first get the single molecule right and then the dimer and trimer in an approximate fashion. Since bulk properties are generally much more accurate than gas-phase properties, the model is fine-tuned for liquid water. After optimization of the parameters the vapor (water clusters) is used as a test case. Like in the N_2 study we have used a shell model. The shell model has a number of advantages over point polarizabilities which makes it attractive in our opinion. First, the equations are simpler and, therefore, computationally cheaper to evaluate than the ones corresponding to point polarizability, especially when one considers grid-based long-range electrostatics methods.[27−29]

* Corresponding author. Tel: 46-18-4714205. Fax: 46-18-511755. E-mail: spoel@xray.bmc.uu.se.

10.1021/jp003843l CCC: $20.00
Published on Web 03/08/2001

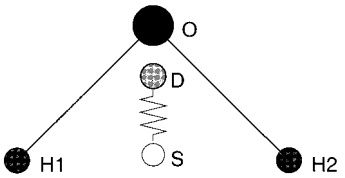

Figure 1. Schematic picture of the SW model: O, oxygen; H, hydrogen; D, dummy; S, shell.

Second, the model corresponds to an intuitive physical picture, that of the electron distribution which shifts in response to an electric field. Finally, when a small Lennard-Jones term is added to the interaction between shell particles and positive charges, the shell model is not affected by the so-called polarizability catastrophe, in which two neighboring polarizabilities polarize one another to become infinitely large.

In this work, we describe new flexible and rigid shell models for water and compare the results of extensive molecular dynamics simulations with these models to simulations employing an earlier shell model by De Leeuw and Parker.[30] Finally, we compare our results with those of several recent polarizable water models taken from the literature.

2. Model and Computational Details Subsection

2.1. Shell-Model Potential. The water model is constructed using the three atoms in the experimental geometry plus a shell particle, representing the electronic degrees of freedom, connected by a spring to a dummy particle located on the bisector of the molecule (Figure 1). Note that the shell particle in this context is not identical to what traditionally has been used in shell models of e.g. ions; such models usually consist of a nucleus and a shell particle which in a vacuum is located on the nucleus.[31] In our model the shell particle is not directly connected to one of the nuclei, but for simplicity we stick with the terminology. By adjusting the charges and the position of the shell particle on the bisector, one can account for the vacuum dipole and quadrupole simultaneously.[32] Polarizability is modeled by allowing the shell particle to move relative to the dummy particle in the field of the surrounding particles, but there is no explicit intramolecular electrostatic interaction like in the LP model.[30] Construction of the dummy particle position and distribution of the force on the dummy particle to the atoms is performed according to ref. 33.

The shell particle is coupled to the dummy particle by either a harmonic spring, yielding isotropic polarizability, or a spring with direction-dependent force constants, yielding anisotropic polarizability. In the first case the force constant k can be related to the polarizability α by writing a balance of forces on the shell particle

$$k\mathbf{r}_{sd} = q_s\boldsymbol{E} \tag{1}$$

where $\boldsymbol{E}$ is the electric field and $\boldsymbol{r}_{sd} = \boldsymbol{r}_s - \boldsymbol{r}_d$ is the vector connecting the shell particle and the dummy particle, combined with

$$\boldsymbol{\mu}_{ind} = \alpha\boldsymbol{E} = q_s\boldsymbol{r}_{sd} \tag{2}$$

where $\boldsymbol{\mu}_{ind}$ is the induced dipole, yielding the following:

$$k = \frac{{q_s}^2}{\alpha} \tag{3}$$

In general α is a tensor but for water the only experimentally determined components are those on the diagonal, (α_{xx}, α_{yy}, α_{zz}), where the coordinate axes are in the molecular frame in which the bisector is on the z axis and the hydrogens are in the yz plane. These terms can be related to three spring constants k_{xx}, k_{yy}, and k_{zz}, respectively, governing motion of the shell particle in each of the respective directions:

$$k_{nn} = \frac{{q_s}^2}{\alpha_{nn}} \tag{4}$$

Here nn is either one of xx, yy, or zz. In the isotropic case we have taken α to be the average of the three diagonal components of the polarizability tensor. The experimental data are listed in Table 1, and the charges, dummy particle position, and spring constants in Table 2.

TABLE 1: Properties of the Water Monomer: Bond Length (nm) and Angle (deg), Vacuum Dipole μ_{vac} (D), and Quadrupole (D Å) with Respect to the Center of Mass θ and Polarizability Volume α (Å^3, Isotropic and Anisotropic)

r_{OH}	0.09572	∠HOH	104.52
μ_{vac}	1.85	α_{iso}	1.470
θ_{xx}	−2.50	α_{xx}	1.415
θ_{yy}	2.63	α_{yy}	1.528
θ_{zz}	−0.13	α_{zz}	1.468

TABLE 2: Charges q (e), Dummy Particle Position ROS (nm), and Isotropic and Anisotropic Spring Constants (kJ/mol^{-1} nm^{-2}) Corresponding to the Shell Particle Charge q_S, Bond Stretching Force Constant k_{OH} (kJ mol^{-1} nm^{-2}), and Angle-Bending Force Constant k_{HOH} (kJ mol^{-1} rad^{-2}), Both from Ref 43

q_O	1.245 88	k_{xx}	608 069
q_H	0.621 34	k_{yy}	563 101
q_S	−2.488 56	k_{zz}	586 116
r_{OS}	0.013 740 8	k_{iso}	585 318
k_{OH}	458 148	k_{HOH}	417.6

When molecular dynamics simulations are performed, the shell particles can be treated in two distinct ways. The most rigorous method is by performing an energy minimization of the shell particle positions at every time step, to ensure that the force on every shell particle is zero. This algorithm enforces the physical fact that the system is always in the ground state with respect to the electronic degrees of freedom. Since it is very time-consuming, two alternatives have been used: prediction and minimization at every Nth step only[13] (typically $N = 5$); giving the shell particle a small mass (typically 0.2 au) and not minimize it at all.[34,35] In this work we have used the most rigorous way of minimization at every step in order to avoid artifacts due to such approximations.

2.2. Parametrization. After determining the charges and spring constants corresponding to the polarizabilities (Table 2), we have to describe the repulsion and dispersion interactions. Popular choices for these interactions are the Lennard-Jones or Buckingham potentials. We have chosen to use the Lennard-Jones 6−12 representation because it is computationally more efficient, because it has fewer parameters, and because the Buckingham potential has a singularity at zero distance which can be problematic when minimizing shell particle positions. In principle one can define up to four atom types in our water model, oxygen (O), hydrogen (H), shell (S), and dummy (D). However, it is advantageous to exclude the dummy particle since the number of interaction sites is reduced from 5 to 4 and the number of interactions is reduced by the square of that ratio, a factor of 1.56. With three particle types left (oxygen, hydrogen, shell) the number of parameters can at most be 12 when a full parameter matrix is used. Ideally, one wants to use as few

TABLE 3: Initial (Unoptimized) Lennard-Jones Parameters C_6 (kJ mol^{-1} nm^{-6}) and C_{12} (kJ mol^{-1} nm^{-12}) for SW

	C_6	C_{12}
O−O	2×10^{-3}	1×10^{-6}
O−S	1×10^{-6}	1×10^{-12}
H−S	4×10^{-5}	2×10^{-8}
H−H	4×10^{-5}	4×10^{-8}

parameters as possible and to use combination rules to calculate the interaction parameters between different atoms. With some trial and error we found an initial set of parameters that gave reasonable energy and conformations for both the water dimer and the water trimer, as compared to experimental data[36] and ab initio calculations.[37,38] The main Lennard-Jones interaction is between the oxygen atoms, but we were not able to get dimer properties in agreement with experimental data without invoking Lennard-Jones interactions between the shell particle and the hydrogen atom and between the hydrogen atoms. The latter in particular was essential to get the orientation of the molecules in the dimer correct. We also added a small Lennard-Jones well to the O−S interaction to avoid the singularity in the Coulomb potential at zero distance. This initial parameter set (Table 3) was then subject to parameter coupling simulation[39,40] which we described in detail in our previous work.[11] We kept the initial C_6 parameter for all interactions; together they are roughly equivalent to the dispersion (C_6) term in other water models such as SPC.[12] The C_{12} parameters for the S−H and the O−O interactions were optimized in parameter coupling simulations of 250 ps. The force field parameters were coupled to the pressure and heat of vaporization ΔH_{vap} as we did in our previous work.[11] ΔH_{vap} can be computed according to[41]

$$\Delta H_{vap} = (E_{intra}(g) + kT) - (E_{intra}(l) + E_i(l)) \qquad (5)$$

where E_i represents the intermolecular energy of the system (which is kT in the gas phase). Since we have pure harmonic potentials for bond stretching and angle bending, the intramolecular energy $E_{intra}(g) = {}^3/_2 kT$, such that

$$\Delta H_{vap} = \frac{5}{2}kT - E_{pot} \qquad (6)$$

For the rigid models the intramolecular energy is zero by definition such that

$$\Delta H_{vap} = kT - E_{pot} \qquad (7)$$

The target E_{pot} for parameter optimization hence was −41.7 kJ/mol for the rigid models[42] and −37.96 kJ/mol for the flexible models at $T = 300$ K. In case of nonharmonic intramolecular potentials, the gas-phase intramolecular energy can be determined by a separate gas-phase simulation.[43]

Optimized parameter sets were determined for flexible and rigid models, each with either anisotropic (AI) or isotropic (ISO) polarizability. We named the models SW-FLEX-AI, SW-FLEX-ISO, SW-RIGID-AI, and SW-RIGID-ISO, respectively. The contraints in the rigid model were handled by the SETTLE algorithm.[44] A cutoff r_c of 0.9 nm for the Lennard-Jones interactions was combined with the particle mesh Ewald algorithm[28] for Coulomb interactions. Long-range dispersion corrections[45] were used in all parametrization and production simulations. The resulting parameter set consists of four different Lennard-Jones interactions, summarized in Tables 3 and 4.

2.3. Simulation Details. Production simulations were run with 820 water molecules in cubic boxes. Minimization of the shell particle positions was performed at each time step of 0.5 fs (flexible) or 1 fs (rigid), with an average of 5 (flexible) to 6 (rigid) force evaluations/time step. A further production run was performed with the LP model.[30] This simulation utilized a time step of 0.2 fs without minimization of the shell particle positions and was 1.3 ns long. The PME method was used here as well. From each simulation the first 50 ps was disregarded as equilibration. The total length of the production simulations are given in Table 5. In all liquid simulations the temperature was controlled by the weak coupling algorithm[46] with $\tau_T = 0.1$ ps and $T_0 = 300$ K. The pressure was controlled in the same manner with $\tau_P = 5$ ps and $P_0 = 1$ bar. All production and parametrization simulations as well as simulation analyses were performed with the GROMACS package.[47,48]

TABLE 4: Optimized Lennard-Jones C_{12} (kJ mol^{-1} nm^{-12}) for SW and Other Parameters As Given in Table 3

	FLEX-AI	RIGID-AI
O−O	1.189×10^{-6}	1.174×10^{-6}
H−S	2.910×10^{-8}	2.766×10^{-8}
	FLEX-ISO	RIGID-ISO
O−O	1.187×10^{-6}	1.176×10^{-6}
H−S	2.937×10^{-8}	2.769×10^{-8}

3. Results

In the following section we describe the results of production simulations of liquid water with our new SW potentials as well as the LP model and of small water clusters for which either experimental data or accurate ab initio calculations are available. In the SW liquid simulations equilibration was monitored by plotting potential energy and density (data not shown). After 50 ps these curves for the SW potentials had leveled off, and the remaining parts of the simulations were used for analysis. Of the LP simulation we used the interval from 50 to 1000 ps for comparison with the SW simulations (but see details below).

3.1. Thermodynamic Properties. The potential energy E_{pot} and the density ρ at 300 K are reproduced very well in the new SW models (see Table 5). The average pressure is close to one in all simulations, but the fluctuations are larger than for nonpolarizable models simulated with a cutoff or a reaction field.[11] It is not clear whether the difference is due to the PME algorithm, to the polarizability, or to the intramolecular flexibility although the fluctuations are slightly lower for the rigid models than for the flexible ones. Energy and density fluctuations are comparable to nonpolarizable potentials. In conclusion this means that the SW models reproduce the observables they were fit to in unrestrained simulations.

3.2. Liquid Structure. The O−O radial distribution function $g_{OO}(r)$ is plotted in Figure 2 for SW-FLEX-AI and SW-RIGID-AI. The $g_{OO}(r)$ for the isotropic models were nearly identical to those of anisotropic models and were left out for clarity. Both g_{OO} have a broad first maximum at 0.29 nm; the second (at 0.53 nm) and third (at 0.7 nm) peaks are not very pronounced. In comparison with experiment,[49,50] the SW potentials have higher first peaks at larger distances.

To get an indication of the range of dipole−dipole correlation effects we have plotted the distance dependent dipole − dipole correlation for the SW-PME-AI model, defined as

$$h_{OO}(r) = 3g_{OO}(r)\langle \cos\theta \rangle \qquad (8)$$

where θ is the angle between the dipoles of water molecules at oxygen−oxygen distance r (Figure 3). This function is related

TABLE 5: Observables of the SW Potentials in the Liquid Phase: Temperature T (K), E_{pot} (kJ mol^{-1}), Density ρ (g/L), Pressure P (bar), Dielectric Constant ϵ, Debye Relaxation Time τ_D (ps), and Self-Diffusion Constant D (10^{-5} cm^2 s^{-1})[a]

model	no. of mol	length	T	E_{pot}	r	P	e	τ_D	D
SWFLEX-AI	820	1300	300	−41.72(0.18)[b]	997(4)	2(670)	116(15)	7.3	3.66(0.19)
SWFLEX-ISO	820	1200	300	−41.69(0.17)[b]	997(8)	5(670)	118(10)	7.9	3.58(0.02)
SWRIGID-AI	820	1550	300	−41.69(0.16)	996(3)	0(480)	97(8)	7.3	3.22(0.15)
SWRIGID-ISO	820	1550	300	−41.68(0.16)	993(3)	1(490)	100(15)	5.6	3.30(0.34)
LP	820	1300	300	−45.10(0.48)	1298(22)	−6(820)	109(19)	3.4	0.85
TIP4PFQ	256	1000	298	−41.4	1000	0.0	79(8)	8	1.9
Dang	550	200	298	−41.17(0.29)	995(7)	1.013			2.1(0.1)
RER(pol)	216	50	300	−41.2	1000	−200			2.8
PPC	256	300−500	298	−41.4	997		77	8.9	2.6
SPC-pol-1	100	c	298	−41.6[d]	1066(2)		98(6)[d]		
TIP4P-pol-3	100	c	298	−41.1[d]	995(2)		69(12)[d]		
MCDHO	1000	e	298	−43.5[d]	1020(10)				
Expt				−41.7[f]	997[g]		78[h]	8.3[h]	2.3[i]

[a] Results are compared to those of the LP potential[30] (this work) and values from literature for the following models: TIP4P−FQ;[22] Dang;[20] RER(pol);[17] PPC;[19] SPC-pol-1, TIP4P-pol-3,[21] MDCHO;[64] Experimental data. The simulation length is given in picoseconds. [b] A constant of $^3/_2kT$ (3.742 kJ mol^{-1}) was subtracted from E_{pot} to facilitate comparison with rigid models. [c] 3×10^6 Monte Carlo moves. [d] Determined in constant-volume Monte Carlo simulations at the experimental density. [e] 2.5×10^8 Monte Carlo moves. [f] Reference 42. [g] Reference 83. [h] References 84−86. [i] References 54 and 55.

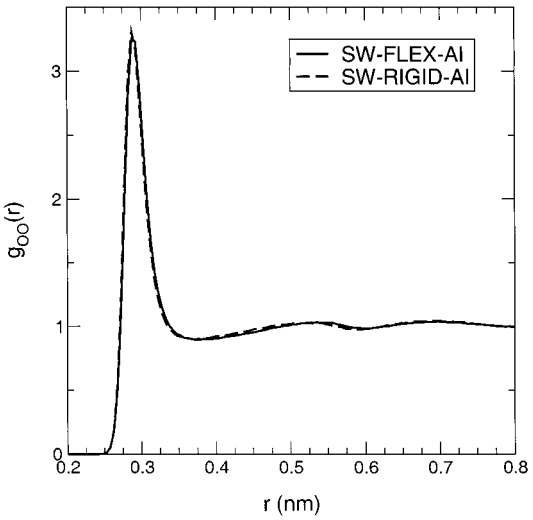

Figure 2. Oxygen−oxygen radial distribution function from the SW-FLEX-AI and SW-RIGID-AI simulationS.

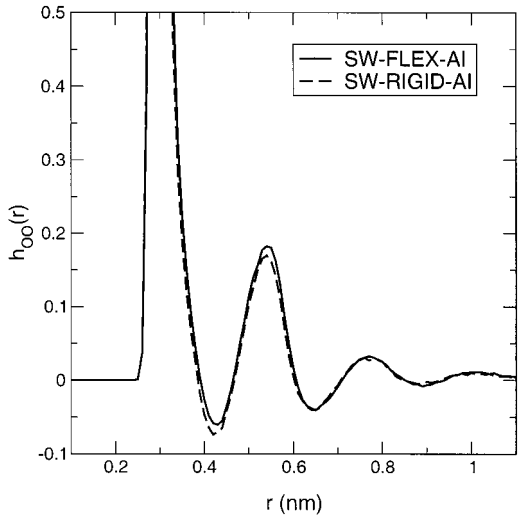

Figure 3. Distance-dependent dipole−dipole correlation function for SW-FLEX-AI and SW-RIGID-AI.

to the possibly more familiar distance-dependent Kirkwood factor $G_k(r)$[51] by[52]

$$G_k(r) = 1 + \frac{4\pi N_p}{3V}\int_0^r r^2 h_{OO}(r)\,dr = \sum_{r_{ij}<r}\frac{\boldsymbol{\mu}_i\cdot\boldsymbol{\mu}_j}{\langle\boldsymbol{\mu}\rangle^2} \qquad (9)$$

where $\boldsymbol{\mu}_i$ and $\boldsymbol{\mu}_j$ are the dipole vectors of water molecules. It can be seen that $h_{OO}(r)$ converges to 0 slower than the $g_{OO}(r)$ goes to 1, indicating that the orientational correlation in the liquid is considerably longer than what is evident from the RDF, as was observed previously.[11,53] The difference between flexible and rigid models is very small, the peaks move inward slightly (0.002 nm) in the rigid models, but the heights of the peaks are virtually identical.

3.3. Water Dynamics. Diffusion constants D were calculated from the mean square displacement (MSD) of oxygen atoms through the Einstein relation.[45] The first 100 ps of the MSD was discarded, and D was determined from a fit to a straight line of the remainder of the MSD plots. The results are listed in Table 5. The flexible models yield 10% higher diffusion constant than the rigid ones for both isotropic and anisotropic models. All values are too high compared to the experimental value of 2.3.[54,55]

3.4. Equilibrium Geometry and Induced Dipole Moments. With a flexible model it is possible to analyze the average geometry of water in the condensed phase. We find that the average OH bond length is 0.0968 ± 0.0024 nm in both the SW-FLEX simulations, 1.1% longer than the gas-phase value of 0.095 72 nm. The average HOH angle is 102.7 ± 0.1°, roughly 1.7% smaller than the gas-phase value of 104.52°. The average dipoles of the SW water molecules are 2.69 (FLEX-AI), 2.68 (FLEX-ISO), and 2.61 (RIGID-AI and RIGID-ISO). Clearly, the flexible models are more polarizable because bond-stretching as well as reduction of the angle leads to a larger dipole. The distribution of dipole moments (Figure 4) approximates a Gaussian centered around 2.68 D with σ 0.2 D (FLEX-AI) and 2.61 D with σ 0.16 (RIGID-AI), respectively. Extremes for FLEX-AI were 1.67 and 3.64 D and for RIGID-AI 1.87 and 3.27 D. The polarization of the flexible model is thus clearly different from the rigid, with higher average dipole and wider distribution. We have also determined the angular distribution of induced dipoles. The mean angle between the permanent and the induced dipole is roughly 12° in all SW simulations, considerably lower than previous estimates from polarizable water models,[13,18] which were around 20°.

3.5. Dielectric Properties. The dielectric constant ϵ of liquid water can be determined from the fluctuations in the total dipole

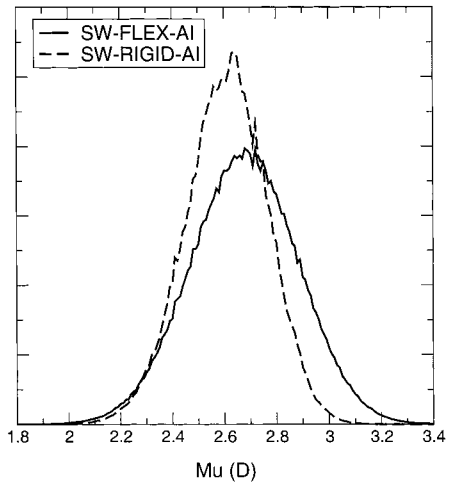

Figure 4. Distribution of dipole moments in the SW-FLEX-AI and SW-RIGID-AI simulations.

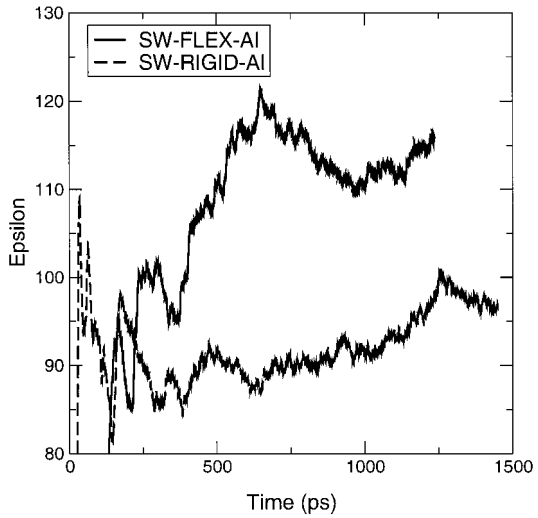

Figure 5. Convergence of the dielectric constant in the SW-FLEX-AI and SW-RIGID-AI simulations.

moment $\mathbf{M}$[56] using a Claussius−Mosotti type expression:

$$\frac{\epsilon - 1}{3}\frac{2\epsilon_{rf} + 1}{2\epsilon_{rf} + \epsilon} = \frac{\langle \mathbf{M}^2 \rangle - \langle \mathbf{M} \rangle^2}{9\epsilon_0 V k_B T} \tag{10}$$

where ϵ_0 is the permittivity of vacuum, V is the volume, and k_B is Boltzmann's constant. Since we assume conducting boundary conditions $\epsilon_{rf} = \infty$, and eq 10 reduces to

$$\epsilon = 1 + \frac{\langle \mathbf{M}^2 \rangle - \langle \mathbf{M} \rangle^2}{3\epsilon_0 V k_B T} \tag{11}$$

The results are plotted in Figure 5 for FLEX-AI and RIGID-AI and listed for all simulations in Table 5. In general the average dipole $\langle \mathbf{M} \rangle$ should converge to zero, but this may require very long simulation times, up to 1 order of magnitude longer than we have done here.[57] The error in the dielectric constant was estimated by cutting the trajectories in bits of roughly 300 ps and computing the standard deviation of the dielectric constants obtained from these bits. For the SW models the standard deviations were between 8% and 15%, whereas it was 18% for the LP model. The resulting errors are given in Table 5.

3.6. Water Clusters. *3.6.1. Water Dimer*. The energy and geometry of the water dimer are summarized in Table 6. Besides the experimental data, we give numbers for several popular water models such as TIP4P,[58] SPC/E,[6] the flexible model of Ferguson,[43] and the shell model of de Leeuw and Parker (LP).[30] The computed O−O distance, the minimum energy of the SW models, and the geometry are all within the experimental error margins, and the dipole is very close to the ab initio value. The nonpolarizable models TIP4P, SPC/E, and Ferguson do not behave as well in the gas phase, which is to be expected as the these models are parametrized for reproducing liquid water properties rather than cluster properties.

TABLE 6: Comparison of Water Dimer Properties. Oxygen−Oxygen Distance R_{OO} (nm), Minimum Potential Energy E_{pot} (kJ mol^{-1}), Donor Angle θ_d (deg), Acceptor Angle θ_a (deg), and Total Dipole Moment of the Dimer μ (D)[a]

model	R_{OO}	θ_d[b]	θ_a[b]	E_{pot}	m
SWFLEX-AI	0.295	56.2	55.2	−21.78	2.59
SWFLEX-ISO	0.295	54.5	56.9	−21.75	2.65
SWRIGID-AI	0.294	59.2	59.1	−21.91	2.55
SWRIGID-ISO	0.293	56.7	56.3	−21.91	2.47
LP	0.297	50.7	32.0	−20.2	2.96
TIP4P	0.274	53.6	49.8	−26.35	2.70
SPC/E	0.274	52.3	21.5	−30.1	3.76
Ferguson	0.274	50.6	21.8	−28.75	3.78
TIP4PFQ	0.292			−18.8	
Dang	0.287			−19.62	
RER(pol)	0.295	47	19	−14.7	
PPC	0.281	51	25.5	−24.1	
SPC-pol-1	0.288	52.5	14.1	−20.9	
TIP4P-pol-3	0.277	54.9	40.2	−22.2	
MCDHO	0.292	57.0	56.1	−20.9	2.68
ab initio	0.291	55.6	57.9	−21.0	
expt	0.295[c]	57(10)[d]	51(10)[d]	−22.6(3)[e]	2.60[f]

[a] Results are given for the SW Potentials, the LP model[30] and the non-polarizable models TIP4P,[58] SPC/E,[6] and Ferguson[43] (all done in this work). For reference literature values for the polarizable models TIP4P−FQ,[22] Dang,[20] RER(pol),[17] PPC,[19] SPC-pol-1 and TIP4P-pol-3,[21] and MCDHO[64] are given, alongside with the most recent ab initio results[66] and experimental data. [b] θ_d and θ_a are the angles between the oxygens and the bisector of the donor and acceptor molecule. [c] Reference 37 based on experimental data from ref 36. [d] Reference 36. [e] Reference 87. [f] Reference 36.

3.6.2. Water Trimer and Tetramer. To further test our newly developed SW potentials, we have calculated the minimum energy, total dipole, and average nearest-neighbor O−O distance R_{OO} for clusters of three and four water molecules (Table 7). The SW trimers are very good; the r_{OO} matches the experimental distance,[59] while the energy and dipole are almost identical to ab initio results.[38,60] However since the ab initio r_{OO} does not agree with the experimental value, it is not possible to determine how accurate the energy and dipole are. In case of the tetramer the SW models all have too large r_{OO} as compared to experiment[61] and, somewhat surprising, even larger r_{OO} than in the trimer. The energy is higher than the ab initio results, and in all cases, the total dipole is not equal to zero which means that the system is not symmetric. For comparison we also give values for the previously mentioned water models. As expected, the nonpolarizable models yield very short O−O distances. The TIP4P model[58] is clearly better than the other models and in good agreement with ab initio calculations.[60] Like in the trimer, the ab initio r_{OO} does not agree very well with the experimental value, and therefore, the reliability of the ab initio results from the literature remains unclear.

3.7. Simulation with the LP Potential. To compare our new models with a published shell model, we performed a simulation of 820 molecules using the model of De Leeuw and Parker.[30] In this simulation the energy decreased constantly (Figure 6A)

TABLE 7: Comparison of Water Trimer and Tetramer Properties. Average Oxygen−Oxygen Distance R_{OO} (nm), Minimum Potential Energy E_{pot} (kJ mol^{-1}), and Total Dipole Moment of the Cluster μ (D)[a]

	trimer			tetramer		
model	E_{pot}	m	R_{OO}	E_{pot}	m	R_{OO}
SWFLEX-AI	−64.4	1.14	0.288	−107.2	0.07	0.290
SWFLEX-ISO	−64.3	1.10	0.289	−107.0	0.07	0.290
SWRIGID-AI	−64.1	1.12	0.287	−107.2	0.15	0.288
SWRIGID-ISO	−64.1	1.11	0.287	−107.2	0.12	0.288
LP	−58.0	0.00	0.296	−91.7	0.00	0.294
TIP4P	−70.7	0.55	0.274	−117.8	0.01	0.271
SPC/E	−82.0	0.03	0.274	−136.0	0.02	0.270
Ferguson	−79.2	0.00	0.275	−133.3	0.00	0.270
Dang			0.286			0.278
SPC-pol-1	−59.6		0.288	−112		0.279
TIP4P-pol-3	−61.2		0.277	−114		0.272
MCDHO	−58.5	1.14	0.291	−108.2	0.02	0.281
ab initio[b]	−65.9		0.278	−120		0.274
ab initio[c]	−66.9	1.14	0.279	−119.1	0.00	0.274
expt			0.287[d]			0.280[e]

[a] Results are given for the SW potentials, the LP model,[30] and the nonpolarizable models TIP4P,[58] SPC/E,[6] and Ferguson[43] (all done in this work). For reference, literature values for the polarizable models of Dang,[20] SPC-pol-1 and TIP4P-pol-3,[21] and MDCHO[64] are given, alongside with recent ab initio results and experimental data. [b] Reference 38. [c] Reference 60. [d] Reference 59. [e] Reference 61.

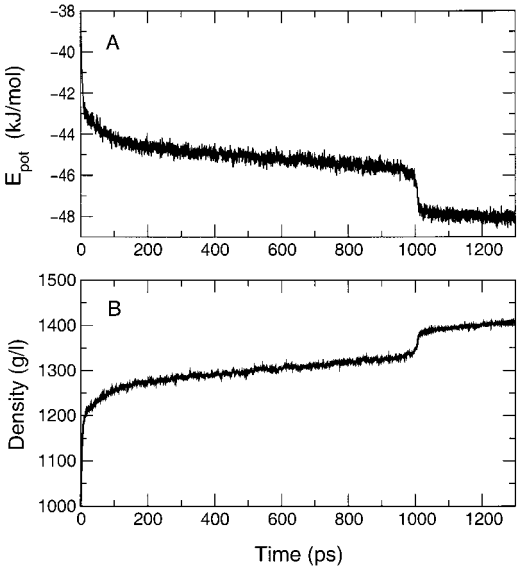

Figure 6. (A) Potential energy and (B) density in the LP simulation. A phase transition is visible at 1000 ps.

while the density increased (Figure 6B). After 1000 ps something akin to a phase change occurred: a sudden drop in energy combined with a density increase. This finding is corroborated by plots of the mean square displacement (Figure 7A) and the oxygen−oxygen radial distribution function (RDF, Figure 7B) at the start and end of the simulation. Diffusion comes to a halt at 1000 ps, and there clearly is increased ordering in the RDF, such that we should conclude that the system freezes after 1000 ps and within a time span of 10 ps. A visual inspection of the conformation at the end of the simulation shows that the molecules pack in hexagonal close packing with O−O distance varying between 0.28 and 0.32 nm (data not shown). As this simulation was performed at 300 K and 1 bar and the density is much too high both in liquid and crystalline state, this behavior is clearly unphysical. However it is still remarkable in the sense that freezing is notoriously difficult to simulate. Simulations of water crystallization reported to date

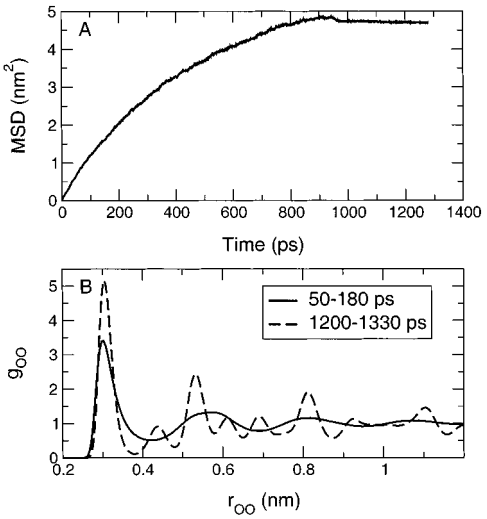

Figure 7. (A) Mean square displacement (MSD) as a function of time in the LP simulation and (B) oxygen−oxygen radial distribution function g_{OO} at the start and at the end of the LP simulation.

all involved an applied external electric field[62,63] and are difficult to reproduce. A further test simulation with the LP potential at 300 K and constant experimental density (997 g/L), starting from a homogeneous density, yielded a single vacuum bubble in the liquid, indicating that the density increased purely due to too strong intermolecular interactions. It seems likely that the phase change in the LP simulation was not detected by the original authors because of their relatively short (100 ps) liquid simulation.

3.8. Comparison with Other Models. To establish the quality of the SW models relative to other polarizable models, we have collected some data from the literature. We have only included potentials for which liquid simulation data were available. Results for the models TIP4P-FQ,[22] Dang,[20] RER(pol),[17] PPC,[19] SPC-pol-1 and TIP4P-pol-3,[21] and MCDHO[64] have been added to Tables 5−7.

3.8.1. Liquid. First of all it should be noted that our simulations are considerably longer than those in the literature and performed with a larger system (except for MCDHO[64]). In Table 5 we see that the SW models, the TIP4P-FQ model,[22] and the PPC model[19] are the only ones to reproduce simultaneously the energy and density of the liquid state at 300 K (note that the TIP4P-FQ and PPC models were optimized to reproduce an energy of −41.4 kJ mol^{-1} at 298 K). Furthermore, the diffusion constants for the SW models are higher than for the other models, which can in part be explained by the larger system size.[11] Finally, the dielectric constant is larger for the SW models than for those in the literature, but considering the system size and simulation lengths, the good correspondence with experiment for the PPC and TIP4P-pol-3[21] models is probably fortuitous. In Figure 5 it can be seen that convergence of the dielectric constant takes at least 1 ns; thus, it is possible that the TIP4P-FQ model[22] indeed does have a dielectric constant close to the experimental value.

3.8.2. Gas Phase. For the water dimer most polarizable models fail to reproduce the water dimer geometry (Table 6), except for the SW models and the MCDHO model,[64] which was fitted on ab initio calculations of the dimer potential energy surface. For the Dang[20] and TIP4P-FQ[22] models no geometry data were published except the oxygen−oxygen distance, and in both cases the energy is too high. It should be noted that we assumed an oxygen−oxygen distance of 0.295 nm in the water dimer when optimizing the potential function, as derived by

van Duijneveldt−van de Rijdt and van Duijneveldt[37] on the basis of the experimental data of Odutola and Dyke.[36] At the time of parametrizing the SW models we were unaware of a paper by Åstrand et al.[65] in which it was argued that the oxygen−oxygen distance more likely is 0.291 nm, which is now confirmed by coupled-cluster calculations of the water dimer.[66] Saint-Martin et al.[64] did use an oxygen−oxygen distance of 0.291 in optimizing their MCDHO potential, and hence, their model performs slightly better than the SW models for the water dimer. The other polarizable models listed all have the acceptor angle too small which implies a too low dipole. In case of the water trimer (Table 7) the SW models are better than the other models, except maybe the SPC-pol-1 model[21] which has a slightly too high energy compared to ab initio calculations. The Dang model[20] also has good oxygen−oxygen distances, but no energy or dipole were available. It is curious that the oxygen−oxygen distance predicted by the MCDHO model[64] is virtually identical to that for the dimer whereas all the other polarizable models have clearly shorter distances. The tetramer is different again; here the SW models have too large oxygen−oxygen distance whereas the MCDHO and SPC-pol-1 both do have reasonable energy and oxygen−oxygen distance.

4. Discussion

It has been suggested[67] that for a good water potential it is necessary to include a feature to describe the directionality of hydrogen bonds, i.e., the tetrahedral structural of water. This feature, well-known from ice, is also apparent in the geometry of the water dimer.[36] The cluster calculations we have presented here (Tables 6 and 7) demonstrate that in our new SW models the relative orientations of molecules in the dimer as well as the trimer are in good agreement with available experimental data.[36,37,59] Although energy and dipole of the trimer are in good agreement with ab initio calculations,[38,60] these in turn fail to reproduce the experimental average O−O distance in the trimer, such that the validity of these results remains undetermined. The tetramers of our new SW models do not seem as compact as they should be compared to experiment.[61] All in all it seems that our SW models perform very well for small clusters, and given that the isolated molecule has perfect dipole, quadrupole, and polarizability by design, we can conclude that the gas phase is well described by our new models.

The imperfections in the average O−O distance in the tetramer also seems to impair the liquid structure of the SW models, as demonstrated by the radial distribution function (RFD, Figure 2). The peaks in the RDF are at too large a distance (0.29 nm), and the second and third peak are not as pronounced as they should be, at least according to the latest neutron diffraction data,[49,50] while recent X-ray diffraction experiments[68] seem to suggest that the first maximum is even further in (at 0.273 nm). It should be noted that the interpretation of neutron diffraction experiments in terms of pair correlation functions has been questioned by Pusztai recently,[69,70] but his interpretation of the available experimental data is controversial as well.[68] Although there is no direct experimental reference for the dipole−dipole correlation (Figure 3), this must also be affected by the short-range order, i.e., the distance between oxygens. One hard experimental fact indicating that the O−O distance should be considerably smaller is the O−O distance in ice I_h, which is 0.275 nm.[71] In line with the suggestion of Stone mentioned above,[67] we think that a good tetrahedral geometry like we have in the SW dimer is probably a prerequisite for a good water model, but it does not automatically imply a proper liquid structure.

A number of other water models, based on either ab initio calculations[72,73] or spectroscopy,[74] have recently been proposed. These models are much more complicated than ours, containing up to 65 parameters, and have hitherto only been tested on water clusters, and they seem to perform very well. The quality of these models for condensed phase simulation has yet to be established. A further model based on ab initio calculations[75] also yields good cluster properties; however, the energy of ice I_h is 6 kJ/mol too low for this model. The MCDHO model,[64] which is discussed in the Results, has good cluster properties, but the liquid energy and density are not as good. It remains therefore unclear whether ab initio methods are accurate enough to build models for condensed phase calculations.

It is evident that the equilibrium molecular geometry in the liquid need not be the same as that in the gas phase. We find that the average HOH angle is somewhat smaller in the liquid than in the gas phase. Experimental evidence for smaller as well as larger angles is present, but the consensus seems to be that the HOH angle in the liquid is within 2° from the gas-phase value of 104.52°.[76] The geometries of the ST2,[77] SPC,[12] and SPC/E[6] models are based on a tetrahedral (109.47°) HOH angle and an OH bond length of 0.1 nm. The latter seems too long compared with our average of 0.0968 nm which in turn is in good agreement with experimental data derived from spectroscopy on ice (0.0972 nm).[78] Since our models are not perfect, in particular at short intermolecular distances (see Figure 2), we cannot draw strong conclusions on the geometry of water in the liquid phase. The average dipole of 2.65 D for the SW models falls well within the estimates for liquid water of 2.6 D[79] to 2.9 ± 0.6 D,[80] but it is lower than the value reported by Dang for his polarizable water model under ambient conditions (2.75 D[81]). In contrast, the average dipoles are considerably higher than that found in a density functional study of 32 water molecules in a cubic box with periodic boundary conditions[82] where a value of 2.43 ± 0.31 D was obtained.

We have investigated the influence of the anisotropy of the polarizability of water by parametrizing isotropically and anisotropically polarizable models and testing these in liquid simulations. The differences are very small, and if anything, the anisotropic models seem to be slightly better behaved than the isotropic ones, with a slightly lower diffusion constant, a slightly lower dielectric constant, and better dimer and trimer properties (Tables 5−7). The difference between flexible and rigid models are more pronounced. The dipole distribution (Figure 4) is narrower, with a smaller average dipole for the rigid models. Furthermore, the diffusion constant as well as the dielectric constant are considerably lower in the rigid models and, hence, closer to experimental data. As we found before in nonpolarizable water simulations,[11] there is a simple relation between mobility and dielectric relaxation, with faster diffusion leading to higher dielectric constants. It seems that the effective polarizability of our models is slightly too low due to the Lennard-Jones interactions, leading to a water molecule that is not "sticky" enough.

In conclusion it seems that our new SW models are very good for the gas phase and satisfatory for the liquid phase; the properties of the SW models are a genuine improvement over the LP model. None of the simple polarizable models that we have reviewed in the results section and in Tables 5−7 (Dang,[20] RER(pol),[17] PPC,[19] and MCDHO[64]) have simultaneously good dimer properties and good liquid properties such as the SW models do. Moreover, only the SW models correctly reproduce the properties of the water monomer. Further refinement of the parameters should lead to a better liquid structure and other

liquid properties, without undoing the good quality of the model for the gas phase. Optimizing with a shorter oxygen−oxygen distance for the dimer will most likely lead to shorter distances in the liquid as well. Since we have optimized only two out of eight possible parameters, there certainly is room for improvement.

Acknowledgment. The authors acknowledge stimulating discussions with Herman Berendsen and Abraham Szöke and a generous gift of computer time by Erik Lindahl. The Swedish research council for engineering sciences (TFR) is acknowledged for project support.

References and Notes

(1) Barron, L. D.; Hecht, L.; Wilson, G. *Biochemistry* **1997**, *36*, 13143−13147.
(2) Wilson, G.; Hecht, L.; Barron, L. D. *Biochemistry* **1996**, *35*, 12518−12525.
(3) van der Spoel, D.; Berendsen, H. J. C. *Biophys. J.* **1997**, *72*, 2032−2041.
(4) Brodsky, A. *Chem. Phys. Lett.* **1996**, *261*, 563−568.
(5) van der Spoel, D.; van Buuren, A. R.; Tieleman, D. P.; Berendsen, H. J. C. *J. Biomol. NMR* **1996**, *8*, 229−238.
(6) Berendsen, H. J. C.; Grigera, J. R.; Straatsma, T. P. *J. Phys. Chem.* **1987**, *91*, 6269−6271.
(7) Kemmink, J.; van Mierlo, C. P. M.; Scheek, R. M.; Creighton, T. E. *J. Mol. Biol.* **1993**, *230*, 312−322.
(8) van Buuren, A. R.; Marrink, S. J.; Berendsen, H. J. C. *J. Phys. Chem.* **1993**, *97*, 9206−9212.
(9) Báez, L. A.; Clancy, P. *J. Chem. Phys.* **1994**, *101*, 9837−9840.
(10) Smith, P. E.; van Gunsteren, W. F. *J. Chem. Phys.* **1994**, *100*, 3169−3174.
(11) van der Spoel, D.; van Maaren, P. J.; Berendsen, H. J. C. *J. Chem. Phys.* **1998**, *108*, 10220−10230.
(12) Berendsen, H. J. C.; Postma, J. P. M.; van Gunsteren, W. F.; Hermans, J. In *Intermolecular Forces*; Pullman, B., Ed.; D. Reidel Publishing Co.: Dordrecht, The Netherlands, 1981; pp 331−342.
(13) Ahlström, P.; Wallqvist, A.; Engström, S.; Jönsson, B. *Mol. Phys.* **1989**, *68*, 563−581.
(14) Cieplak, P.; Kollman, P. A.; Lybrand, T. *J. Chem. Phys.* **1990**, *92*, 6755−6760.
(15) Caldwell, J.; Dang, L. X.; Kollman, P. A. *J. Am. Chem. Soc.* **1990**, *112*, 9144−9147.
(16) Dang, L. X. *J. Chem. Phys.* **1992**, *97*, 2659−2660.
(17) Wallqvist, A.; Berne, B. J. *J. Phys. Chem.* **1993**, *97*, 13841−13851.
(18) Chialvo, A. A.; Cummings, P. T. *J. Chem. Phys.* **1996**, *105*, 8274−8281.
(19) Svishchev, I. M.; Kusalik, P. G.; Wang, J.; Boyd, R. J. *J. Chem. Phys.* **1996**, *105*, 4742−4750.
(20) Dang, L. X.; Chang, T. M. *J. Chem. Phys.* **1997**, *106*, 8149−8159.
(21) Chen, B.; Xing, J. H.; Siepmann, J. I. *J. Phys. Chem. B* **2000**, *104*, 2391−2401.
(22) Rick, S. W.; Stuart, S. J.; Berne, B. J. *J. Chem. Phys.* **1994**, *101*, 6141−6156.
(23) Banks, J. L.; Kaminski, G. A.; Zhou, R. H.; Mainz, D. T.; Berne, B. J.; Friesner, R. A. *J. Chem. Phys.* **1999**, *110*, 741−754.
(24) Jorgensen, W. L.; Tirado-Rives, J. *J. Am. Chem. Soc.* **1988**, *110*, 1657−1666.
(25) Bader, J. S.; Cortis, C. M.; Berne, B. J. *J. Chem. Phys.* **1999**, 2372−2387.
(26) Jordan, P. C.; van Maaren, P. J.; Mavri, J.; van der Spoel, D.; Berendsen, H. J. C. *J. Chem. Phys.* **1995**, *103*, 2272−2285.
(27) Hockney, R. W.; Eastwood, J. W. *Computer simulation using particles;* McGraw-Hill: New York, 1981.
(28) Darden, T.; York, D.; Pedersen, L. *J. Chem. Phys.* **1993**, *98*, 10089−10092.
(29) Toukmaji, A.; Sagui, C.; Board, J.; Darden, T. *J. Chem. Phys.* **2000**, *113*, 10913−10927.
(30) de Leeuw, N. H.; Parker, S. C. *Phys. Rev. B* **1998**, *58*, 13901−13908.
(31) Dick, B. G.; Overhauser, A. W. *Phys. Rev.* **1958**, *112*, 90−103.
(32) Kozack, R. E.; Jordan, P. C. *J. Chem. Phys.* **1992**, *96*, 3120−3130.
(33) Berendsen, H. J. C.; van Gunsteren, W. F. In *Molecular Liquids-Dynamics and Interactions*; A. J. Barnes et al., Eds.; NATO ASI C 135; Reidel: Dordrecht, The Netherlands, 1984; pp 475−500.
(34) Lindan, P. J. D.; Gillan, M. J. *J. Phys.: Condens. Matter* **1993**, *5*, 1019−1030.
(35) Mitchell, P. J.; Fincham, D. *J. Phys.: Condens Matter* **1993**, *5*, 1031−1038.
(36) Odutola, J. A.; Dyke, T. R. *J. Chem. Phys.* **1980**, *72*, 5062−5070.
(37) van Duijneveldt van de Rijdt, J. G. C. M.; van Duijneveldt, F. B. *J. Chem. Phys.* **1992**, *97*, 5019−5030.
(38) Gregory, J. K.; Clary, D. C.; Liu, K.; Brown, M. G.; Saykally, R. J. *Science* **1997**, *275*, 814−817.
(39) Chung, J. W. Force field optimisation using coupling theory. Master's Thesis, University of Groningen, 1993.
(40) Njo, S. L.; Gunsteren, W. F.; Müller-Plathe, F. *J. Chem. Phys.* **1995**, *102*, 6199−6207.
(41) Kaminski, G.; Duffy, E. M.; Matsui, T.; Jorgensen, W. L. *J. Phys. Chem.* **1994**, *98*, 13077−13082.
(42) Postma, J. P. M. A Molecular Dynamics study of water. Ph.D. Thesis, University of Groningen, 1985.
(43) Ferguson, D. M. *J. Comput. Chem.* **1995**, *16*, 501−511.
(44) Miyamoto, S.; Kollman, P. A. *J. Comput. Chem.* **1992**, *13*, 952−962.
(45) Allen, M. P.; Tildesley, D. J. *Computer Simulations of Liquids*; Oxford Science Publications: Oxford, U.K., 1987.
(46) Berendsen, H. J. C.; Postma, J. P. M.; DiNola, A.; Haak, J. R. *J. Chem. Phys.* **1984**, *81*, 3684−3690.
(47) Berendsen, H. J. C.; van der Spoel, D.; van Drunen, R. *Comput. Phys. Commun.* **1995**, *91*, 43−56.
(48) van der Spoel, D.; van Buuren, A. R.; Apol, E.; Meulenhoff, P. J.; Tieleman, D. P.; Sijbers, A. L. T. M.; Hess, B.; Feenstra, K. A.; van Drunen, R.; Berendsen, H. J. C. *Gromacs User Manual version 2.*0; University of Groningen: Nijenborgh 4, 9747 AG Groningen, The Netherlands, 1999. Internet: http://md.chem.rug.nl/∼gmx.
(49) Soper, A. K.; Phillips, M. G. *Chem. Phys.* **1986**, *107*, 47−60.
(50) Soper, A. K.; Bruni, F.; Ricci, M. A. *J. Chem. Phys.* **1997**, *106*, 247−254.
(51) Neumann, M.; Steinhauser, O. *Mol. Phys.* **1980**, *39*, 437−454.
(52) Nymand, T. M.; Linse, P. *J. Chem. Phys.* **2000**, *112*, 6386−6395.
(53) Chipot, C.; Milot, C.; Maigret, B.; Kollman, P. A. *J. Chem. Phys.* **1994**, *101*, 7953−7962.
(54) Krynicki, K.; Green, C. D.; Sawyer, D. W. *Discuss. Faraday Soc.* **1978**, *66*, 199−208.
(55) Price, W. S.; Ide, H.; Arata, Y. *J. Phys. Chem. A* **1999**, *103*, 448−450.
(56) Neumann, M. *Mol. Phys.* **1983**, *50*, 841−858.
(57) van der Spoel, D.; van Maaren, P. J. Manuscript in preparation.
(58) Jorgensen, W. L.; Chandrasekhar, J.; Madura, J. D.; Impey, R. W.; Klein, M. L. *J. Chem. Phys.* **1983**, *79*, 926−935.
(59) Liu, K.; Loeser, J. G.; Elrod, M. J.; Host, B. C.; Rzepiela, J. A.; Pugliano, N.; Saykally, R. J. *J. Am. Chem. Soc.* **1994**, *116*, 3507−3512.
(60) Lee, H. M.; Suh, S. B.; Lee, J. Y.; Tarakeshwar, P.; Kim, K. S. *J. Chem. Phys.* **2000**, *112*, 9759−9772.
(61) Cruzan, J. D.; Braly, L. B.; Liu, K.; Brown, M. G.; Loeser, J. G.; Saykally, R. J. *Science* **1996**, *271*, 59−62.
(62) Svishchev, I. M.; Kusalik, P. G. *Phys. Rev. Lett.* **1994**, *73*, 975−978.
(63) Borzsák, I.; Cummings, P. T. *Phys. Rev.* E **1997**, *56*, R6279−R6282.
(64) Saint-Martin, H.; Hernández-Cobos, J.; Bernal-Uruchurtu, M. I.; Ortega-Blake, I.; Berendsen, H. J. C. *J. Chem. Phys.* **2000**, *113*, 10899−10912.
(65) Åstrand, P. O.; Karlström, G.; Engdahl, A.; Nelander, B. *J. Chem. Phys.* **1995**, *102*, 3534−3554.
(66) Klopper, W.; van Duijneveldt-van de Rijdt, J. G. C. M.; van Duijneveldt, F. B. *Phys. Chem. Chem. Phys.* **2000**, *2*, 2227−2234.
(67) Stone, A. J. *The theory of intermolecular forces*; Clarendon Press: Oxford, U.K., 1996.
(68) Hura, G.; Sorenson, J. M.; Head-Gordon, R. M. G. T. *J. Chem. Phys.* **2000**, *113*, 9140−9148.
(69) Pusztai, L. *Phys. Rev.* B **1999**, *60*, 11851−11854.
(70) Pusztai, L. *Physica* B **2000**, *276*, 419−420.
(71) Kuhs, W. F.; Lehmann, M. S. *J. Phys.* (*Paris*) **1987**, *48*, 3.
(72) Mas, E. M.; Szalewicz, K. *J. Chem. Phys.* **1997**, *107*, 4207−4218.
(73) Groenenboom, G. C.; Mas, E. M.; Bukowski, R.; Szalewicz, K.; Wormer, P. E. S.; van der Avoird, A. *Phys. Rev. Lett.* **2000**, *84*, 4072−4075.
(74) Fellers, R. S.; Leforestier, C.; Braly, L. B.; Brown, M. G.; Saykally, R. J. *Science* **1999**, *284*, 945−948.
(75) Burnham, C. J.; Li, J.; Xantheas, S.; Leslie, M. *J. Chem. Phys.* **1999**, *110*, 4566−4581.
(76) Zhu, S.-B.; Singh, S.; Robinson, G. W. *Adv. Chem. Phys.* **1994**, *85*, 627−731.
(77) Stillinger, F. H.; Rahman, A. *J. Chem. Phys.* **1974**, *60*, 1545−1557.
(78) Whalley, E. *J. Glaciol.* **1978**, *21*, 13−31.
(79) Coulson, C. A.; Eisenberg, D. *Proc. R. Soc. London Ser. A* **1966**, *291*, 445−459.

(80) Baydal, Y. S.; Saboungi, M. L.; Price, D. L.; Shastri, S. D.; Haeffner, D. R. *J. Chem. Phys.* **2000**, *112*, 9206−9208.
(81) Dang, L. X. *J. Phys. Chem. B.* **1998**, *102*, 620−624.
(82) Site, I. D.; Alavi, A.; Lynden-Bell, R. M. *Mol. Phys.* **1999**, *96*, 1683−1693.
(83) Weast, R. C. *Handbook of Chemistry and Physics;* CRC Press: Cleveland, OH, 1977.
(84) Kaatze, U. *J. Chem. Eng. Data* **1989**, *34*, 371−374.
(85) Barthel, J.; Bachhuber, K.; Buchner, R.; Hetzenauer, H. *Chem. Phys. Lett.* **1990**, *165*, 369−373.
(86) Kindt, J. T.; Schmuttenmaer, C. A. *J. Phys. Chem.* **1996**, *100*, 10373−10379.
(87) Curtiss, L. A.; Frurip, D. J.; Blancher, M. *J. Chem. Phys.* **1979**, *71*, 2703−2711.